

promoting access to White Rose research papers



Universities of Leeds, Sheffield and York
<http://eprints.whiterose.ac.uk/>

This is the published version of an article in the **Journal of Geophysical Research D: Atmospheres, 115 (12)**

White Rose Research Online URL for this paper:

<http://eprints.whiterose.ac.uk/id/eprint/76611>

Published article:

Knippertz, P and Todd, MC (2010) *The central west Saharan dust hot spot and its relation to African easterly waves and extratropical disturbances*. Journal of Geophysical Research D: Atmospheres, 115 (12). D12117. ISSN 0148-0227

<http://dx.doi.org/10.1029/2009JD012819>

The central west Saharan dust hot spot and its relation to African easterly waves and extratropical disturbances

Peter Knippertz¹ and Martin C. Todd^{2,3}

Received 13 July 2009; revised 16 February 2010; accepted 23 February 2010; published 23 June 2010.

[1] A vast, arid, and virtually uninhabited region covering eastern Mauritania and northern Mali appears in satellite estimates of dust loading as the global maximum during boreal summer. Here the complex meteorological conditions that create this central western Sahara (CWS) dust hot spot are investigated on the basis of regression analyses and case study examples using a wide range of satellite analysis products. The results confirm the importance of African easterly waves (AEWs), previously hypothesized on the basis of case studies. The main ingredients to create this connection are as follows.

(1) Strengthened southerlies to the east of an AEW trough advect moist air into the southern Sahara. Daytime heating and orography trigger moist convection in this air mass. Strong evaporation in dry midlevel air generates extended cold pools and haboob dust storms. (2) Vertical mixing brings dust into the upper parts of the deep Saharan boundary layer, from where it can be advected back into the CWS region with the northerlies ahead of the next AEW trough. (3) If the associated surface vortex is strong enough, more dust emission occurs within or just upstream of the CWS. (4) High-amplitude waves in the subtropics enhance the meridional flow associated with the AEW. Although there is a considerable case-to-case variability, it can be concluded that AEWs in concert with extratropical disturbances substantially contribute to the hot spot creation both through emission and the organization of transport. Disagreement between different satellite products and the presence of clouds complicate the analysis and underline the necessity for new observations.

Citation: Knippertz, P., and M. C. Todd (2010), The central west Saharan dust hot spot and its relation to African easterly waves and extratropical disturbances, *J. Geophys. Res.*, 115, D12117, doi:10.1029/2009JD012819.

1. Introduction

[2] It is now widely recognized that mineral dust aerosols are an important part of the climate system [Forster *et al.*, 2007]. This is by virtue of the direct effect on the radiation budget [e.g., Haywood *et al.*, 2001], the indirect effect on cloud properties [e.g., Richardson *et al.*, 2007], and the semidirect effect of this on the atmospheric circulation. Dust deposits also influence terrestrial and oceanic ecosystems and therefore the global carbon cycle [e.g., Jickells *et al.*, 2005].

[3] Climatological analyses of atmospheric mineral dust loadings based upon different satellite estimates consistently point to a vast, arid, and virtually uninhabited region in eastern Mauritania and northern Mali as one of the most active hot spots worldwide, particularly during the months of June to September [Brooks and Legrand, 2000; Prospero

et al., 2002; Washington *et al.*, 2003; Engelstaedter *et al.*, 2006]. For the lack of a better terminology the authors will refer to this region as the central western Sahara (CWS) for the rest of this paper. Due to its remote location and hostile climate, the CWS region has only been analyzed on the basis of satellite observations and model experiments. The CWS hot spot is evident in independent satellite products including Aerosol Optical Thickness (AOT) estimates from Multiangle Imaging SpectroRadiometer (MISR) visible data and the Aerosol Indices (AIs) from the Total Ozone Mapping Spectrometer (TOMS) and the Ozone Monitoring Instrument (OMI), which both observe at UV wavelengths (Figure 1; see section 2.1 for more information on the data). It is often assumed that high dust loadings imply collocated strong surface sources. This assumption is probably not justified for most synoptic-scale single emission events, when the strong winds that mobilize the dust also transport it away rather quickly, and might not even be true in a climatological sense for regions with a clear prevalence of wind direction. A possible indication of this problem is the shift in activity maxima over West Africa between some of the long-term satellite aerosol products (compare Figure 3 of Engelstaedter *et al.* [2006] with Figure 2 of Brooks and Legrand [2000]). In fact, a recent 2 year source activation

¹Institute for Climate and Atmospheric Science, School of Earth and Environment, University of Leeds, Leeds, UK.

²Department of Geography, University College London, London, UK.

³Now at Department of Geography, University of Sussex, Brighton, UK.

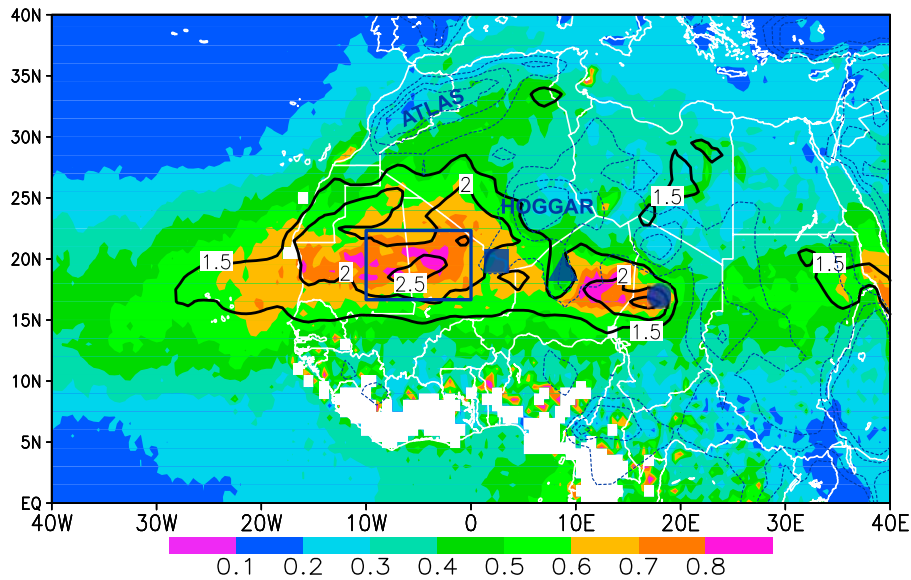


Figure 1. Climatological mean aerosol loading over North Africa during June–September. Mean MISR AOT at 558 nm wavelength 2000–2006 (shading) and mean TOMS AI 1979–1992 (solid contours). Also shown are 500, 750, and 1000 m surface elevation (blue dashed contours) and relevant geographical features (blue box marks central western Sahara region, circle marks Bodélé Depression, triangle marks Air Mountains, and square marks Adrar des Iforas Uplands).

climatology based upon data in 15 min temporal resolution from the Spinning Enhanced Visible and Infrared Imager (SEVIRI) flying on the geostationary Meteosat Second Generation satellites points to regions to the east and north of the CWS as more important dust sources [see *Schepanski et al.*, 2009, Figure 1]. Another issue in this context is the near-noon sampling of some satellites leading to a misrepresentation of sources activated by afternoon convective activity [*Schepanski et al.*, 2007].

[4] While the meteorological mechanisms controlling dust emissions from prominent local sources such as the Bodélé Depression in northern Chad are now much better understood [*Washington and Todd*, 2005; *Washington et al.*, 2006; *Todd et al.*, 2008], the geological, geomorphological, and meteorological reasons that make the vast CWS region such a prominent hot spot are still unclear. *Prospero et al.* [2002] and *Washington et al.* [2003] describe the region as a complex low-relief terrain with few distinctive features, which may have received alluvial deposits from the Niger river and from wadis draining the Hoggar and Adrar des Iforas uplands to the north and east in the past, as indicated by several ancient lake beds. The source activation frequency map of *Schepanski et al.* [2009] does in fact indicate localized sources, associated substantially with surface drainage features, rather than the broad area of high aerosol loadings from the AI and MISR AOT products (Figure 1).

[5] Meteorological processes of potential importance to dust emission in the Sahara range from microscale to continental scale and can be grouped into four different mechanisms: mechanism A, dry boundary layer convection such as dust devils and dust plumes [*Koch and Renno*, 2005; *Ansmann et al.*, 2009]; mechanism B, mesoscale “haboob” dust storms related to the gust fronts of organized convective systems, mostly originating from the Sahel [*Sutton*,

1925; *Lawson*, 1971; *Williams et al.*, 2008]; mechanism C, synoptic-scale emissions related to a downward mixing of momentum from nocturnal low-level jets (LLJs) in the northeasterly harmattan flow [*Knippertz*, 2008]; and mechanism D, strong winds and high turbulence at the leading edge of the southerly monsoon flow (called the Intertropical Discontinuity (ITD)) [*Flamant et al.*, 2007; *Bou Karam et al.*, 2008].

[6] *Engelstaedter and Washington* [2007] investigated the mean annual cycle of dust loading over the CWS region as estimated from the TOMS AI and found a better correlation of dustiness with 10 m wind convergence and gustiness than with mean wind speed. They concluded that this points to a prevalence of small-scale processes (mechanism A). *Marsham et al.* [2008] on the other hand showed a relation between dustiness and downdraft convective potential energy and interpreted this to underline the importance of haboobs (mechanism B). *Knippertz* [2008] argued that the strong diurnal cycle involved in mechanism C can create a close relationship between gustiness and dust on the meso-scale and synoptic scale in agreement with the analysis of the diurnal cycle of dust plume emissions by *Schepanski et al.* [2009]. There is a clear need to better understand these individual processes and their relative importance, not least to evaluate the fidelity of the aerosol components of climate models.

[7] Synoptic-scale variability over West Africa during summer is dominated by African Easterly Waves (AEWs) [*Burpee*, 1974; *Kiladis et al.*, 2006, and references therein]. Previous work based upon case studies [*Karyampudi and Carlson*, 1988; *Westphal et al.*, 1988; *Karyampudi et al.*, 1999] and dust model simulations driven by analyzed wind fields [*Jones et al.*, 2003] has shown that AEWs modify dustiness over the downstream eastern Atlantic. For the dust generation in the CWS region itself, *Knippertz*

[2008] discusses impacts of occasional shifts of the position of the heat trough over West Africa related to extratropical disturbances. The precise role of AEWs in this process remains to be determined. Possible mechanisms relating AEWs and dust emission are variations in the near-surface pressure that lead to stronger nighttime accelerations toward the pressure trough (mechanisms C and D) or by favoring the occurrence of haboob dust storms at the southern margin of the Sahara through the northward advection of moisture (mechanism B) [Fink and Reiner, 2003].

[8] The aim of this paper is to provide the most comprehensive analysis of the association of AEWs and extratropical disturbances with dust generation over the CWS region conducted to date. Unlike previous studies, this will be achieved by statistical analysis of long-term satellite aerosol and meteorological products (section 3) and through detailed analysis of representative case study events (section 4). The main objective is to assess the relative importance of mechanisms B–D as explained above and to better understand their relation to AEWs. A meaningful assessment of mechanism A is difficult to make from the available data. In addition, section 2 contains a description of the employed data and methods, and section 5 provides a discussion of the results and the main conclusions.

2. Data and Methods

[9] Understanding the association of AEWs with dust generation and transport is strongly aided by observational data with extensive space/time coverage. The only such source of information on aerosols over the CWS is satellite data. In this study we utilize a number of independent, long-term satellite aerosol products to ensure robust results from statistical analysis. To provide insights into atmospheric controls on dust mechanisms the day-to-day variability in the aerosol loading over the CWS in conjunction with information on the state of the atmosphere is examined. Our approach here is to undertake a self-consistent analysis of both (1) the generalized statistical association of CWS dust variability and the large-scale circulation from long-term data (section 3) and (2) detailed analysis of case studies objectively selected from these same aerosol data (section 4).

2.1. Observational Data

[10] Three different types of satellite data are used in this study. The AI from TOMS and OMI is derived from the spectral contrast of measurements in two UV channels (340 nm and 380 nm) providing a dimensionless index, which has been shown to have an approximately linear relationship to the column AOT for smoke and dust aerosols [Herman *et al.*, 1997; Hsu *et al.*, 1999; Torres *et al.*, 2007; Christopher *et al.*, 2008]. Over summertime West Africa the AI predominantly reflects dust, but smaller contributions from other aerosols cannot be excluded. Both OMI and TOMS AI are sensitive to the vertical distribution of the aerosol. There is an ongoing debate about how well the AI is able to capture dust below about 1.5 km [Herman and Celarier, 1997; Torres *et al.*, 2002]. The potential height bias would underestimate atmospheric dust content in regions with low-level dust transport or a shallow boundary layer [Mahowald and Dufresne, 2004]. The TOMS AI covers the period 1979–1992 at 1.25° longitude by 1° lati-

tude resolution, whilst the OMI AI product covers the period 2005–2007 with a resolution of 0.25°. The higher resolution of OMI substantially reduces, but certainly does not eliminate, the likelihood of subpixel cloud contamination [Ahn *et al.*, 2008].

[11] The second data set used is retrievals of AOT at 558 nm wavelength from MISR onboard the National Aeronautic and Space Administration (NASA) Terra spacecraft with a local equatorial crossing time of 1030 h. MISR observes the Earth using nine cameras distributed at different angles in four wavelengths, allowing quantification of tropospheric aerosols [Bothwell *et al.*, 2002]. The spatial resolution is about 20 km but the narrow swath limits the temporal resolution to around one week, impeding a robust statistical analysis of the relationship with the large-scale atmospheric circulation on a daily basis. Here the 0.5° daily gridded product for 2000–2007 is used.

[12] For the case studies in section 4 we employ a fairly new (available since 2004) product based on brightness temperatures (BTs) from three SEVIRI infrared (IR) channels. These images are composited using BT differences 10.8 μm minus 12.0 μm for red, 10.8 μm minus 8.7 μm for green, and BTs at 10.8 μm for blue (for more details see http://oiswww.eumetsat.org/WEBOPS/msg_interpretation/atmospheric_constituents.php). Although this product only provides a qualitative estimate of dust loading, the high temporal resolution of 15 min allows a detailed analysis of dust emission and transport [Schepanski *et al.*, 2007]. It is particularly suited to detect freshly emitted dust due to the sensitivity of IR channels to the existence of a coarse mode [Sokolik *et al.*, 1998]. The red color in these images is closely related to dust particle size, while the blue color is more sensitive to dust optical depth [Li *et al.*, 2007]. A decrease in IR signals relative to products based on shorter wavelengths (such as OMI) with transport distance has been observed [Pierangelo *et al.*, 2004]. In contrast to OMI, most IR techniques including the SEVIRI dust product are not very sensitive to dust layer height [Wald *et al.*, 1998]. There is, however, a sensitivity of the employed IR channels to water vapor, which leads to problems with detecting dust over the moist southern parts of West Africa in summer [Chaboureau *et al.*, 2007; Flamant *et al.*, 2007].

[13] Information on the state of the atmosphere was obtained from two independent reanalysis products, the National Center for Environmental Prediction (NCEP) reanalysis (daily means, 2.5° grid, 1979–2007 [Kalnay *et al.*, 1996]) and the European Centre for Medium-Range Weather Forecasts (ECMWF) ERA-Interim reanalysis (1200 UTC fields, 1° grid, 1989–2007 [Uppala *et al.*, 2008]). Atmospheric fields of geopotential height and winds at 1000 hPa and 700 hPa, and specific humidity at 1000 hPa were chosen to enable diagnosis of AEW activity and controls on dust emission and convection. In addition, satellite outgoing longwave radiation (OLR) observations from the National Oceanic and Atmospheric Administration (NOAA; 2.5° daily mean [Liebmann and Smith, 1996]) were employed as a proxy for deep convection over the region. For the case studies in section 4 operational ECMWF analyses of 1200 UTC mean sea-level pressure (MSLP) and its anomalies with respect to long-term monthly means were used.

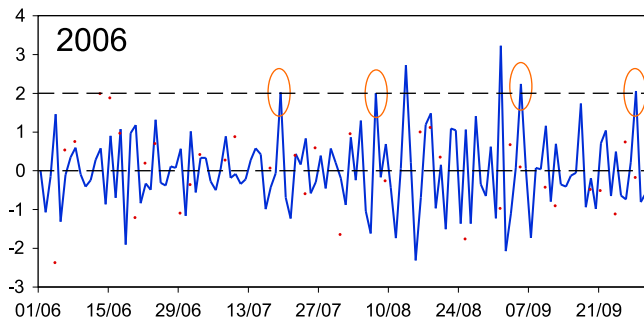


Figure 2. Time series of $AI(OMI)_{CWS}$ (blue line) and AOT_{CWS} (red dots) for boreal summer 2006 (dates given as dd/mm). The 2 standard deviation line and the four events studied in section 4 are marked. For more details on how the indices are computed, see section 2.

2.2. Time Series Generation

[14] Daily time series of AI from TOMS and OMI, and MISR AOT for the CWS region were created by averaging the gridded satellite products over the region $16^{\circ}N$ – $22^{\circ}N$, 0° – $10^{\circ}W$, broadly encompassing the zone of mean maximum aerosol loading during June–September in both the AI and MISR AOT products (blue box in Figure 1). The narrow swath of MISR precludes full coverage of this region during one overpass and therefore only those satellite passes with more than 25% coverage were included in creating the daily area average to ensure representative sampling. For each time series daily anomalies were calculated with respect to the 30 day running mean of the daily climatology (i.e., the mean of each day averaged over the period of the particular data record). These daily anomalies were then standardized separately for each data type (TOMS, OMI and MISR) by dividing by the standard deviation of daily anomalies for that particular data set. This way the resulting time series are comparable between the different sensors. In the case of TOMS and OMI AIs, high-pass filtering was applied to retain variance at time scales less than 10 days associated with synoptic-scale disturbances (irregular temporal sampling from MISR precludes time filtering). Data for the months June–September were then extracted for statistical analysis. These time series, hereafter referred to as $AI(TOMS)_{CWS}$, $AI(OMI)_{CWS}$, and AOT_{CWS} , represent the standardized variability in dust over the CWS over extended periods. The time series for boreal summer 2006 is shown in Figure 2, and forms the basis of the selection of case study events in section 4. Note that the poor temporal and spatial sampling of MISR together with the time filtering applied to the OMI data make a comparison between the two time series difficult.

2.3. Method

[15] The association of AEWs and CWS dust is determined by projecting the atmospheric fields onto the dust time series by linear regression. This method has been successfully applied to dynamical structures in the tropical atmosphere including AEWs in many previous studies [Kiladis and Wheeler, 1995; Kiladis et al., 2006]. The time series of the dynamical field (technically the predictand, e.g., NCEP 1000 hPa geopotential height) at each grid cell within a wider North African/European domain is first converted to daily

anomalies with respect to the 30 day running mean of the climatological value (1961–1990) and then filtered to retain high-frequency variance at time scales less than 10 days. These gridded anomaly time series are then regressed against the CWS dust time series (technically the predictor, e.g., $AI(OMI)_{CWS}$). The resulting regression coefficients at each grid cell represent the linear dependence of the predictand at that location on variability in the aerosol loading over the CWS region. Using regressions, in which the predictand leads or lags the predictor by -5 to $+5$ days, the time evolution of the anomalies can be inferred. In the following text our notation is such that LAG-3 refers to the regression where the atmospheric field lead the aerosol time series by 3 days. The results can then be presented as maps of the anomalies in the large-scale dynamical field associated with a particular perturbation in aerosol over CWS, in this case $+2$ standard deviations. We will refer to these as “representative perturbations” for the rest of the paper. This term is chosen to indicate that the shown circulation anomalies are not associated with specific real events but represent conditions associated with “typical” major dust outbreaks (see Figure 2). Statistical significance (at the 0.05 level) at each grid cell is determined from the correlation coefficient of the two time series.

[16] The real cases studied in section 4 complement this analysis. Specific examples of major CWS dust events are identified from the time series of $AI(OMI)_{CWS}$, specifically those events greater in magnitude than $+2$ standard deviations. These are then analyzed independently to reveal the involved specific circulation structures. Unlike the bulk statistical analysis described above the case study analysis is able to utilize high-resolution (but qualitative) information on dust emission from the SEVIRI instrument, to reveal the role of mesoscale circulation features and their relationship to the broader structures of AEWs.

3. Statistical Relationship of Dust and Atmospheric Circulation

[17] The bulk statistical relationships between CWS aerosol load and the large-scale circulation are quite insensitive to the choice of reanalysis data and aerosol product. We therefore present only results for the combination of data with the greatest temporal coverage, namely the TOMS AI and NCEP reanalyses during 1979–1992. Conditions where other data give substantially different results are highlighted. Figure 3 shows a time-longitude plot of geopotential height anomalies at 1000 and 700 hPa along 15° – $20^{\circ}N$ associated with a representative perturbation in $AI(TOMS)_{CWS}$. The former level was chosen for its importance for dust mobilization, while 700 hPa reflects both AEW activity and upper-level disturbances from the extratropics. The time dimension here is derived from the lag/lead regression of the aerosol time series and atmospheric data. The results clearly indicate a westward propagation of alternating positive and negative geopotential anomalies over the West African domain ($10^{\circ}E$ – $20^{\circ}W$) during the period leading and following the aerosol anomaly over the CWS with a propagation speed of approximately 800 km d^{-1} (around 9 m s^{-1}) and a wavelength of around 3500 km. The 700 hPa trough is displaced eastward (i.e., upstream) relative to 1000 hPa, indicative of low-level baroclinicity. Such a structure is characteristic of AEW

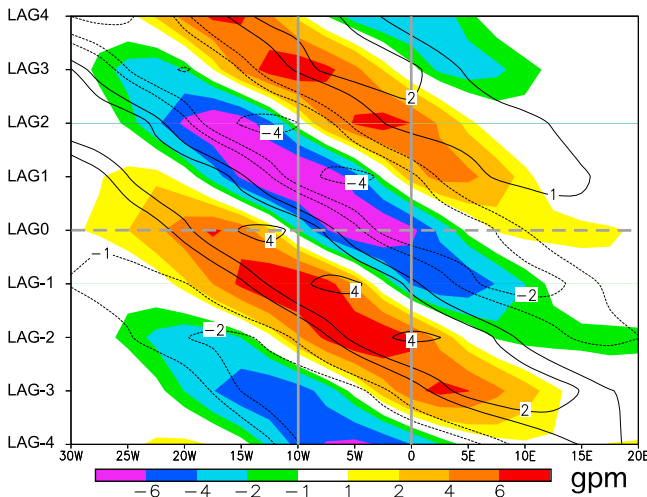


Figure 3. Time-longitude plot of perturbation in geopotential height (15°N – 20°N) associated with a +2 standard deviation in high-pass filtered TOMS AI averaged over the CWS region (marked with grey lines). Shading is 1000 hPa, while contours show 700 hPa. All analysis is based on daily data during June–September for 1979–1992.

activity centered on 15°N in the study of *Kiladis et al.* [2006]. With zero lag in the regression analysis, the CWS region lies within or just to the west of the AEW low-level trough and in the northerly sector at 700 hPa. This basic structure is essentially the same for analysis of all the other aerosol data used (OMI AI and MISR AOT, not shown) and can therefore be considered a robust result. Regressions of $\text{AI}(\text{TOMS})_{\text{CWS}}$ ($\text{AI}(\text{OMI})_{\text{CWS}}$) against TOMS (OMI) AI anomalies averaged over 15°N – 20°N give evidence of a dust signal propagating across the CWS from about 5°E (not shown). This suggests a contribution from dust emission from sources to the east of the CWS associated with the propagating AEW. This issue is considered in more detail below. The poor temporal sampling of MISR precludes a usefully regression of AOT_{CWS} against gridded AOT.

[18] Figure 4 shows the equivalent results as latitude-longitude maps for LAG-3 to LAG0, presenting geopotential height and wind at 1000 and 700 hPa with the former overlaid by specific humidity anomalies and the latter by satellite OLR anomalies. For LAG-3, a clear and statistically significant signal in 1000 hPa geopotential height is found (Figure 4a). The anomalies over West Africa show the typical structure of an AEW with a negative anomaly of about 7 gpm centered near 16°N , 12.5°W and a positive anomaly of similar shape and magnitude about 16° farther east. The corresponding low-latitude anomalies at 700 hPa are shifted eastward by several degrees longitude, reflecting the low-level baroclinic structure of the waves (Figure 4b). Particularly at this higher level the AEW trough is connected with a pronounced extratropical negative geopotential height anomaly with a center over the Canary Islands. LAG-4 maps indicate an origin of this anomaly over the Iberian Peninsula (not shown). Together the two disturbances create an extended region of strong southerly flow that stretches from the Gulf of Guinea to the southern side of the Atlas Mountains. This flow significantly enhances the moisture content over western Niger and northern Mali (red line in Figure 4a), mainly to the east of

the study region (marked with a box in Figure 4). A conspicuous negative OLR anomaly over the western part of the moist anomaly indicates enhanced convective activity (red line in Figure 4b). Anomaly wind vectors at 1000 hPa indicate a highly ageostrophic and divergent flow out of this region toward the northwest indicative of convective downdrafts (Figure 4a). Anomalous wind speeds are higher than in other parts of the AEW structure and point to some potential for dust emission. These results are consistent with an enhanced haboob activity in the moist southerly sector of the wave (mechanism B from section 1), which is strengthened through the interaction with the extratropical disturbance. The affected regions have been identified to be preferred dust sources due to fluvial deposits on the western and southern slopes of the Air, Hoggar and Adrar des Iforas massifs [*Schepanski et al.*, 2009]. Certainly, details cannot be expected to be well resolved in the coarse-resolution data used here, but the net effects in a statistical sense are likely reflected in both wind analyses and OLR measurements. Presumably most dust detection methods from satellites will have problems to identify the associated emissions due to cloud contamination (see the discussion on this subject by *Williams* [2008]).

[19] The same images for LAG-2 show the westward propagation of the wave structure, a weakening of the negative anomalies over the west coast of West Africa, and the emergence of an upstream AEW trough over southern Chad (Figures 4c and 4d). The AEW ridge at 700 hPa, which has now entered the study region from the east, shows a strong connection to a high geopotential region over the Iberian Peninsula and the adjacent western Mediterranean Sea, again leading to extended regions of meridional flow anomalies. The area of negative OLR anomalies, positive specific humidity anomalies, and strong southerly wind anomalies at 1000 hPa has moved into the study region (Figures 4c and 4d), but haboob-related dust emissions, if they occur, are again most likely undetectable from satellites due to cloud cover. OMI data indicate more dust emissions within the northerly 1000 hPa wind anomaly over Niger and Chad (not shown). The analysis for LAG-1 (Figures 4e and 4f) is almost a mirror image of LAG-3. The AEW surface ridge is now located over southern Mali and connected with a high geopotential anomaly over northwestern Africa, while the upstream trough lies over Niger. In between there is a region with strong northerly 1000 hPa wind anomalies from southern Algeria to northern Togo, which is probably associated with dust emission in its northern parts. There are still indications for potential haboob activity just to the west of the study region. The easterly anomalies over northern Niger at both levels are likely to help transporting dust, which has been emitted farther east on the previous day, toward the CWS.

[20] Finally for LAG0, the AEW ridge has propagated to the Mauritanian Atlantic coast, while the upstream trough reaches Mali (Figures 4g and 4h). Both show connections to subtropical features of equal sign, particularly at 700 hPa, creating extended areas of anomalous meridional flow. Low-level wind anomalies peak in the northerlies around the intensified AEW vortex, i.e., right over the study region and to the south of it. The vectors are clearly less ageostrophic than for LAG-1, LAG-2 and LAG-3, but are of a comparable magnitude so that additional dust emission can

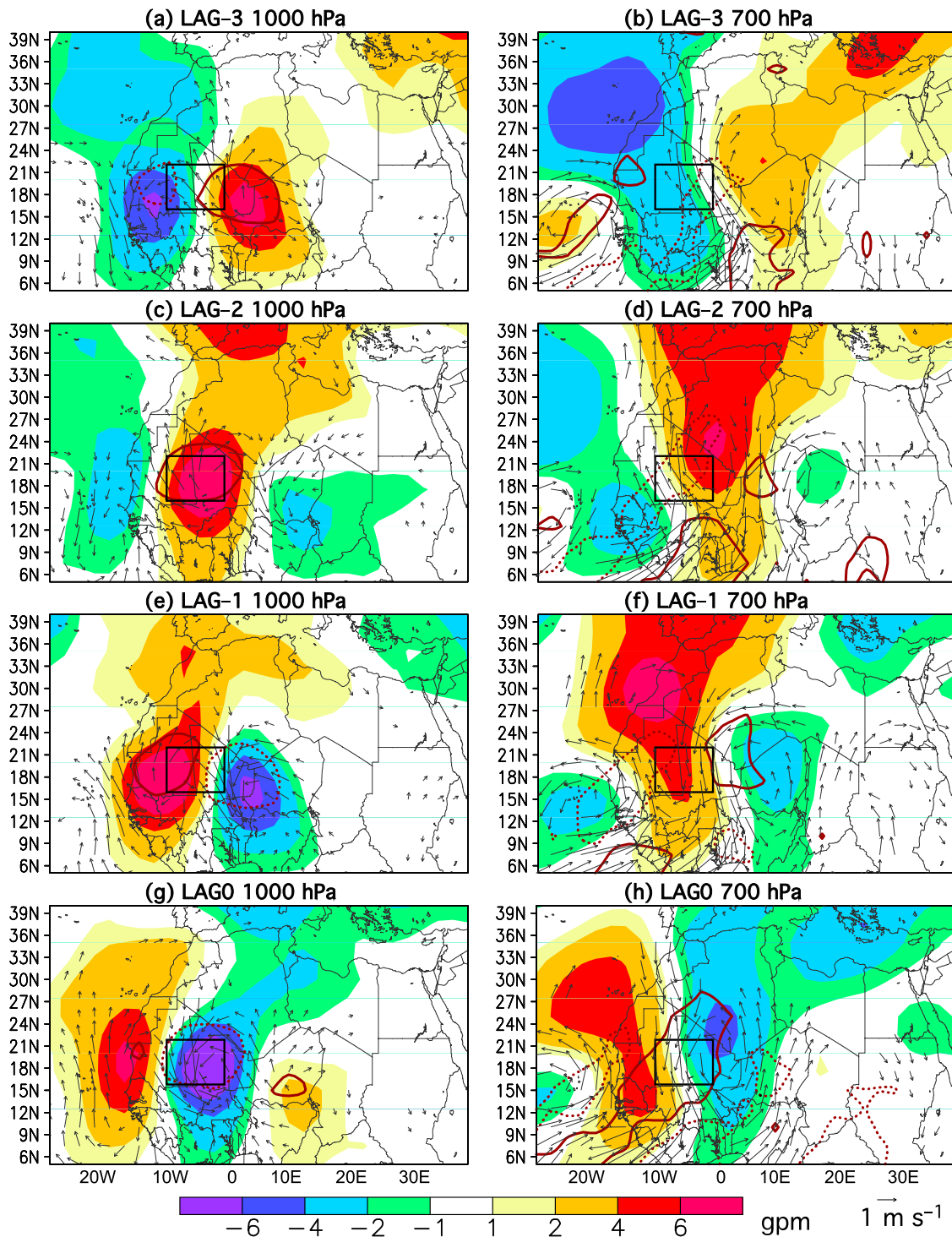


Figure 4. Perturbation in dynamical fields associated with a +2 standard deviation in high-pass filtered TOMS AI averaged over the CWS region (black boxes). (a, c, e, and g) The 1000 hPa geopotential height anomalies with wind perturbations and specific humidity (-0.4 g kg^{-1} (dotted contour) and $+0.4 \text{ g kg}^{-1}$ (solid contour)). (b, d, f, and h) Same as Figures 4a, 4c, 4e, and 4g but for 700 hPa and contours showing OLR perturbations (-4 W m^{-2} (dotted contour) and $+4 \text{ W m}^{-2}$ (solid contour)). For winds, humidity, and OLR, only statistically significant perturbations are shown. Each row corresponds to a different lag relative to the $\text{AI(TOMS)}_{\text{CWS}}$. All analysis is based on daily data during June–September for 1979–1992.

be expected. This pattern is consistent with mechanism C from section 1. The strong northerlies at 700 hPa from the Atlas Mountains toward the Guinea Coast (Figure 4h) might advect some of the dust, which has been mobilized in the AEW southerly sector and then mixed to higher levels, back into the study region, where it contributes to the high $AI(TOMS)_{CWS}$ values. This process would be particularly effective, if a detection of dust below 1.5 km is problematic as has been suggested [Herman and Celarier, 1997; Mahowald and Dufresne, 2004]. As an interesting side remark it is noted that the positive geopotential anomaly in the subtropics moves faster westward than the low-latitude AEW disturbances (Figures 4b, 4d, 4f, and 4h). LAG0 is also characterized by negative specific humidity and very strong positive OLR anomalies over the study region that suggest cloud-free conditions (red lines in Figures 4g and 4h). Given that TOMS has a rather large view of sensor (50 by 50 km at nadir), resulting in a high likelihood of subpixel cloud contamination, highest AI values are presumably biased toward cloud-free conditions and therefore toward the northerly sectors of AEWs.

[21] The picture that emerges from these results suggests a clear association of dustiness over the CWS region and AEWs. The connection involves dust emission from multiple sources over the CWS and upstream resulting from different mesoscale to synoptic-scale processes. AEWs act to both initiate dust emission and to organize subsequent transport into the CWS region. We hypothesize that this occurs as follows.

[22] 1. Haboobs in the southerly sector of an AEW mobilize dust within and to the east of the CWS region in the period up to 3 days prior to the CWS dust peak. This dust is transported northward by the haboob outflow embedded in the large-scale southerlies associated with the AEW and subsequently is mixed into the upper parts of the Saharan boundary layer.

[23] 2. In the following northerly sector, dust is re-advected westward and southward into the CWS and more emission takes place in the CWS region itself and upstream in connection with the AEW cyclonic surface vortex, most likely involving the LLJ mechanism.

[24] 3. The meridional extent of the southerly and northerly sectors are increased by interactions with extratropical disturbances.

[25] 4. Enhanced cloudiness associated with item 1 potentially creates a bias in the satellite estimates of dust toward item 2.

4. Case Study Examples

[26] To further illustrate the statistical results discussed in section 3, detailed case studies of four marked dust events over the CWS region will be presented that exemplify typical synoptic situations. The cases are all taken from the period of June–September 2006, for which both OMI AI and SEVIRI dust data are available. The four cases have the third to sixth largest daily OMI anomalies over the CWS for this period and therefore constitute significant events (Figure 2). The two top events (12 and 31 August 2006) are not shown because of widespread cloud cover over the Sahara prior to the peak in OMI AI. Both cases, however, do share many common features with the four cases presented here.

[27] For a discussion of the relation to the larger-scale circulation, 1000 hPa wind fields for 1200 UTC on the days under study are shown. The 8 g kg^{-1} specific humidity contour at 1000 hPa is used to delineate the northern edge of the moist monsoonal air. This value is closely related to a 2 m dew point of 11°C and therefore slightly drier than standard ITD definitions that use the 14°C or 15°C contour [e.g., Bou Karam et al. 2008].

4.1. A Strong AEW Cyclonic Vortex

[28] From 17 to 18 July 2006 the $AI(OMI)_{CWS}$ increased from -0.07 to 2.02 units, the fifth highest value of the period June–September 2006 (Figure 2). Around midday on 17 July 2006, low-level winds show a distinct cyclonic vortex centered over eastern Mali (Figure 5b). This feature causes northerly flow over large parts of the CWS region. Despite the missing anticyclonic circulation over the coast, the situation has some resemblance to the structures identified in the statistical analysis (Figure 4g) and can therefore serve as an illustration of a typical case.

[29] Animations of SEVIRI images (see auxiliary material Animation S1) show the emergence of major dust plumes from the paleolake deposits of Taoudenni in northern Mali (23°N , 4°W) around 1000 UTC on 17 July.¹ These plumes intensify and spread southwestward in the course of the day (see feature A in Figure 5a for the situation at 1330 UTC). This evolution is consistent with ECMWF analyses, which show an increase in both mean wind and gustiness near the surface from morning to midday (not shown), suggesting a relation to the LLJ mechanism [see Schepanski et al., 2009]. The OMI signal (Figure 5b) also highlights feature A, but additionally indicates widespread dustiness over large parts of Mauritania (feature B). Considering the OMI height bias and the larger sensitivity to smaller particles (see section 2.1), this suggests that this dust was emitted over the previous days and has been mixed to the top of the Saharan boundary layer. The higher moisture contents closer to the coast (red line in Figure 5b) might also contribute to a weaker SEVIRI signal.

[30] To the east of the vortex center southwesterlies reach across eastern Mali to the Algerian border leading to a bulge in the 8 g kg^{-1} specific humidity contour (Figure 5b; see also the corresponding divide between brighter and darker colors in Figure 5a). Farther south, there is strong convective activity in the southerlies (feature C in Figure 5a), which might have supported the northward push of the ITD through the emergence of convective cold pools [Flamant et al., 2009]. A similar, yet weaker pattern is found over eastern Nigeria and eastern Niger (feature D in Figure 5a).

[31] In the course of the afternoon and evening of 17 July, deep convection forms along the southwestern border of Algeria and moves into northern Mali in the course of the night (see auxiliary material Animation S1). This convection generates westward propagating cold pools, which activate dust over the CWS. In the morning of 18 July, further emission from the Taoudenni deposits occur, creating a region of large signals for dust in both SEVIRI and OMI by midday (feature E in Figures 5c and 5d; note the slight downstream shift in the OMI data, which might be related to

¹Auxiliary materials are available in the HTML. doi:10.1029/2009JD012819.

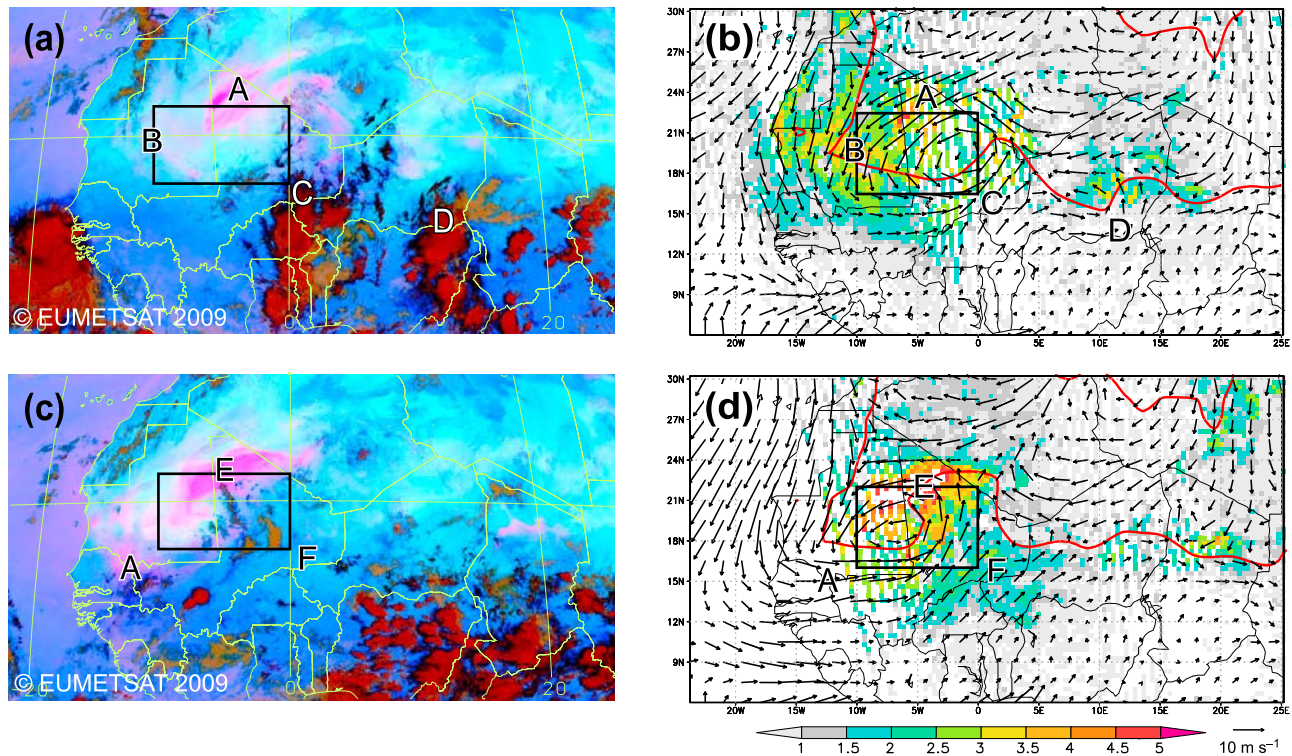


Figure 5. Dustiness and low-level circulation during 17–18 July 2006. (a) SEVIRI dust product and (b) OMI AI at 1330 UTC 17 July 2006. Dust appears in pink and high clouds in red colors. In Figure 5b, vectors are 1000 hPa winds and the thick red line is the 8 g kg^{-1} specific humidity contour at 1000 hPa used to delineate the northern edge of the moist monsoonal air. Both are taken from ECMWF operational analyses at 1200 UTC. (c and d) Same as Figures 5a and 5b but for 18 July 2006. Black boxes mark the study region, and letters label cloud or dust features referred to in the text. Note the difference in map projection between SEVIRI and OMI images.

the height bias). Dust feature A has already reached the eastern border of Senegal by this time. The 1000 hPa winds at 1200 UTC 18 July indicate that the vortex has propagated westward to the border of Mali with Mauritania without a significant change to the wind pattern (Figure 5d). The northward extension of moist monsoonal air is much larger now and covers most of northern Mali. The SEVIRI product clearly struggles to highlight dust in this region (compare feature F in Figures 5c and 5d).

[32] One day later, the 1000 hPa vortex center lies over western Mauritania (not shown) indicating a propagation of about $6\text{--}7^\circ$ longitude per day. This suggests that the cyclonic circulation is the surface reflection of the northern vortex of an AEW, which typically has propagation velocities of this order [Burpee, 1974]. More evidence that AEW activity is present during this period is the fairly large-scale organization of convection seen in Figure 5a. The exact dynamical reasons why the surface vortex is so strong in this case (MSLP anomalies reach 3 and 4 hPa on 17 and 18 July compared to 1.1 hPa for a composite by Burpee [1974]) is beyond the scope of the present paper, but will be subject of future work.

[33] This case illustrates how an AEW trough passing through the CWS can generate dust in both the strong northeasterly winds to the northwest of the cyclonic center and through convective cold pools in the moist southerly flow to the east. This dust is subsequently transported over the CWS in northeasterly flow. These conditions are broadly

consistent with the bulk statistical analysis discussed in section 3.

4.2. A Subtropical Wave

[34] The example of 26–27 September 2006 is characterized by an increase in $\text{AI}(\text{OMI})_{\text{CWS}}$ from 0.22 to 2.05 units, the latter being the fourth highest value during the entire summer. On both days dust emission takes place in the strong northeasterly flow across the study region, to the north of the ITD (see Figure 6 and auxiliary material Animation S2). Strongest activity from morning to midday points to an importance of the LLJ mechanism as in the previous case. The plumes appear to emerge from localized sources in the extreme south of Algeria on 26 September and from northern Mali on the next day (feature A in Figures 6a and 6b). Again there is a downstream shift between the SEVIRI and OMI signals. MISR AOT (not shown) confirms much of the AI structure underlying the qualitative nature of the SEVIRI product, which also does not indicate the strong increase from 26 to 27 September evident from OMI AI. It is not clear to what extent these discrepancies reflect OMI vertical bias and/or SEVIRI sensitivity to particle size and moisture. The comparably cloud-free conditions in the northerlies agree with the statistical results in section 3 (see positive OLR anomaly in Figure 4g) and make cloud contamination an unlikely reason for the large differences to the SEVIRI product.

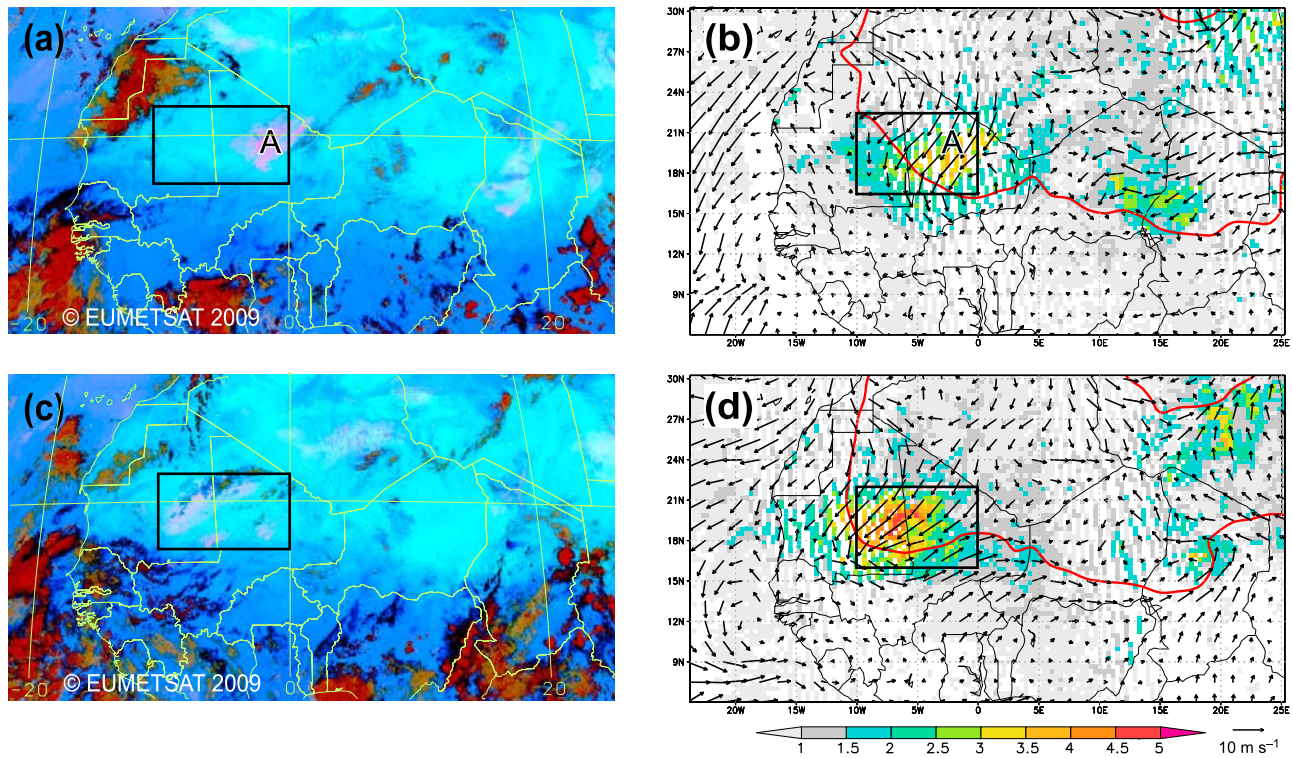


Figure 6. Same as Figure 5 but for 26–27 September 2006.

[35] The northeasterly flow across the CWS in Figures 6b and 6d is in good agreement with the statistical results for LAG0 (see section 3). However, in contrast to these results and to the example discussed in section 4.1, there is little indication of a cyclonic vortex and the 8 g kg^{-1} specific humidity contour is only slightly deformed, suggesting weak AEW activity during this period. Instead, the strong northerlies across Algeria and Mali, which cause most of the dust emission, are related to a wave in the subtropics. It is associated with a strengthening and southeastward excursion of the subtropical high into West Africa, and with the development of a surface depression over the Central Mediterranean, which extends a low-pressure zone across Libya well into the tropics (Figure 7). MSLP anomalies associated with this pattern reach +4 hPa over Mauritania and -8 hPa over the Libyan coast. The unusually high amplitude of this wave appears to be related to the presence of ex-hurricane Helene (45°N , 23°W [see, e.g., Davis *et al.*, 2008]), which was already weakening on 26 September, but had a core pressure of 968 hPa on the previous day (not shown). This case illustrates how synoptic-scale pressure fluctuations in the subtropics can cause dustiness in the CWS region.

4.3. A Hybrid Case

[36] Another significant dust event with an increase in $\text{AI}(\text{OMI})_{\text{CWS}}$ from 0.07 to 2.24 units (third highest value of June–September 2006) occurred during 3–4 September 2006. The evolution is in some sense a hybrid of the cases discussed in sections 4.1 and 4.2 and also shows good agreement with the bulk regression results in section 3. Wind vectors at 1000 hPa indicate a cyclonic vortex, whose center propagates westward from eastern Mali/western Niger to central

Mali by 4 September (Figures 8b and 8d). This feature is associated with MSLP anomalies of -4 and -2 hPa (not shown). Particularly on 4 September, there are strong winds all around the vortex, but again dust emission is most intense in the easterlies to the north of the center from sources in southern Algeria (feature A in Figures 8c and 8d).

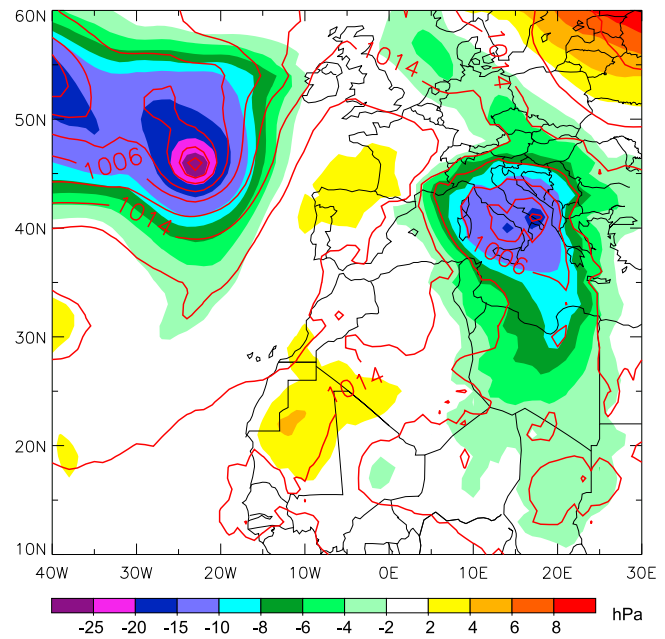


Figure 7. MSLP (red contours every 4 hPa) and the pertinent anomalies with respect to long-term monthly means (shading) for 1200 UTC 26 September 2006.

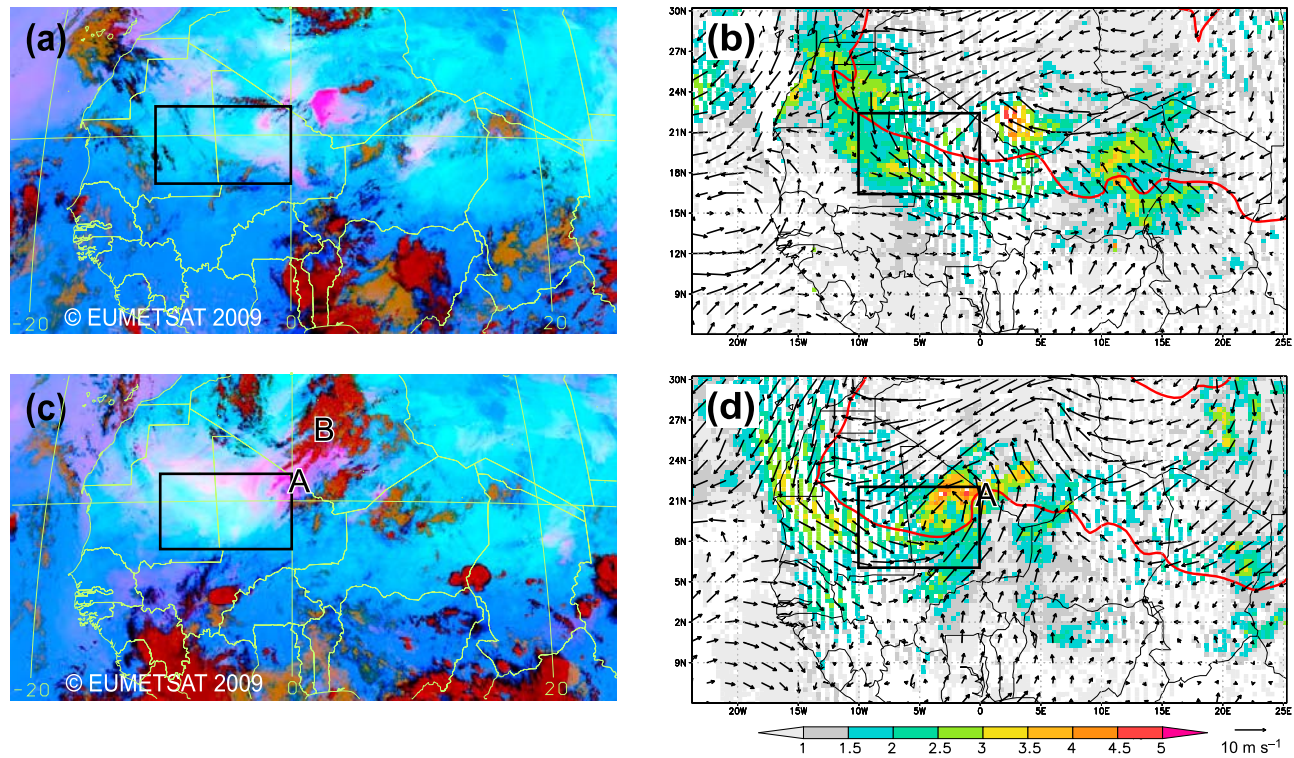


Figure 8. Same as Figure 5 but for 3–4 September 2006.

The accelerated flow over the Sahara is related to anomalously high MSLP over the Mediterranean region (not shown), which enhances the south-north pressure gradient. An increase in dust activity in the morning hours evident from the SEVIRI data points to an importance of LLJs (see auxiliary material Animation S3). In addition, moist air is advected northward to the east of the AEW vortex with southerlies reaching far into southern Algeria. The SEVIRI images show deep convection there (feature B in Figure 8c), but do not reveal to what extent the dust mobilization is due to the strong background flow or through cold pools. Again the SEVIRI signal is shifted upstream with respect to OMI AI and does not show the strong increase on day 2 of the dust event. This case illustrates how tropical and extratropical disturbances can act in concert to enhance dustiness in the CWS region.

4.4. A Monsoon Surge

[37] The last example is a significant dust event that deviates somewhat from the picture evolving from the statistical analysis in section 3. Between 5 and 6 August 2006 the $AI(OMI)_{CWS}$ jumped from -1.62 to 2.00 units, the sixth highest value of the period June–September 2006 (Figure 2). An animation of SEVIRI images show that the dust outbreak begins in connection with the gust fronts of two massive convective systems that form over eastern Mali and western Niger in the early afternoon of 3 August, and then rapidly intensify and merge until midnight (see auxiliary material Animation S4). There is some agreement between this real case and the representative perturbation used in the statistical analysis in section 3, as LAG-3 equally shows indications for convection in this area (Figure 4b).

[38] By midday on 4 August (should be compared to LAG-2) the remnants of the western convective system have reached western Mali (feature A in Figure 9a), while the SEVIRI dust signal shows a very pronounced convex maximum stretching from northern Mali across southern Algeria into northern Niger (feature B), similar to a case investigated by *Westphal et al.* [1988]. There is a substantial northward excursion of moist air and strong southwesterly flow to the east of a cyclonic circulation center over Mauritania (Figure 9b), whose size, strength, and propagation over the previous days suggest the surface signature of an AEW trough. This northward surge of the monsoon is supported by a high-amplitude wave in the extratropics. The MSLP chart for 4 August shows a low-pressure system over the Atlantic, a strongly deformed subtropical high stretching toward the British Isles, and low pressure over the Mediterranean Sea and adjacent Africa (Figure 10). The juxtaposition of the AEW trough (MSLP anomaly of -7 hPa) with an extratropical low over Tunisia (anomaly of -9 hPa) creates the pressure gradients necessary for the meridionally extended region of southerly flow that advects moisture and dust into Algeria.

[39] In the afternoon of 4 August several smaller convective cells form within this air mass (see auxiliary material Animation S4), the remnants of which are still evident in the satellite image at 1330 UTC on 5 August (Figure 9c). These systems generate their own rather small and short-lived cold pools and thereby contribute more dust to the widespread maximum covering large parts of the central Sahara on 5 August (feature C in Figures 9c and 9d). The cyclonic center is still located over Mauritania, slightly farther west than on the previous day, and the northward extension of the moist southwesterly flow is now even more pronounced (Figure 9d).

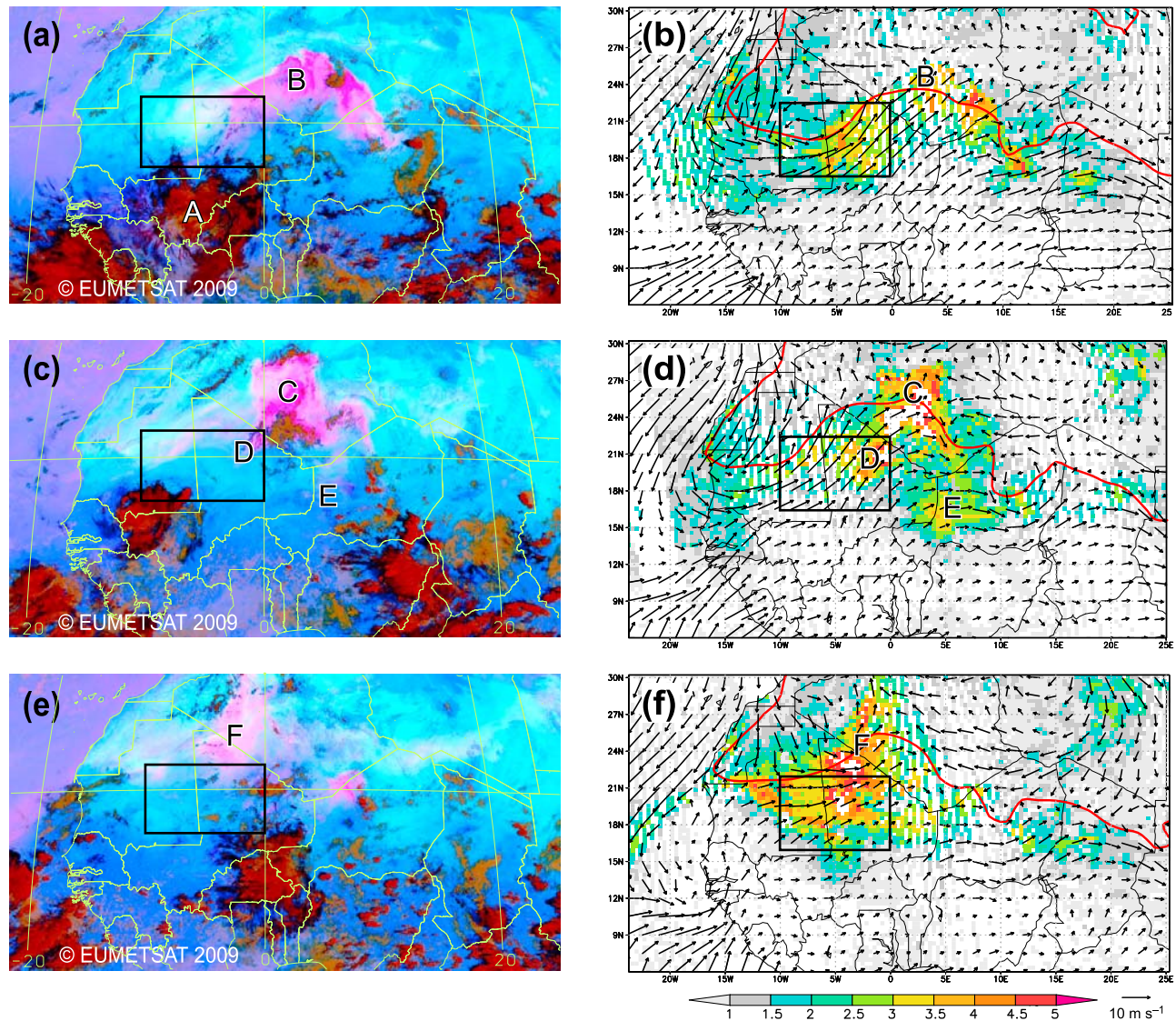


Figure 9. (a–d) Same as Figure 5 but for 4–5 August 2006. (e and f) Corresponding images for 6 August 2006.

Although the SEVIRI images for 4 and 5 August suggest comparable dustiness, the corresponding OMI AI distributions indicate a marked increase as in previous cases. The OMI AI signals over northern Mali and western Niger (features D and E in Figure 9) are not matched by SEVIRI, possibly indicating the presence of aged dust in these regions or SEVIRI bias in moist air. Unfortunately there are no MISR data in this region to confirm the OMI signal.

[40] By midday of 6 August the cyclonic center has moved from Mauritania to western Algeria, still associated with southwesterly or southerly flow over large parts of the western Sahara and a northward shifted moist zone (Figure 9f). This is clearly not in agreement with the regression results for LAG0 in Figure 4g. The unusual track and slow propagation of the cyclonic center together with the very extended southerly sector is not compatible with the typical evolution of an AEW and is presumably closely related to the disturbance by the extratropical circulation. The dust signal weakens in the SEVIRI product on 6 August and slowly drifts westward

into northern Mali and western Algeria (feature F in Figure 9e), while the OMI AI reaches extremely high values farther downstream over the almost cloud-free study region (Figure 9f). This discrepancy is similar to that observed the previous day. Notably, on 6 August the MISR AOT data confirm the high OMI AI south within the moist zone, suggesting that SEVIRI is underrepresenting dust in these conditions.

[41] This case demonstrates how the complex interaction of convective, AEW, and synoptic activity in the subtropics can act together to generate a strong dust event over the CWS involving several mechanisms discussed in this paper, most notably haboob events upstream of the CWS.

5. Summary and Conclusions

[42] The broad central west Saharan (CWS) region centered around 19°N, 5°W appears in most satellite products to have the highest dust loadings anywhere in the world during

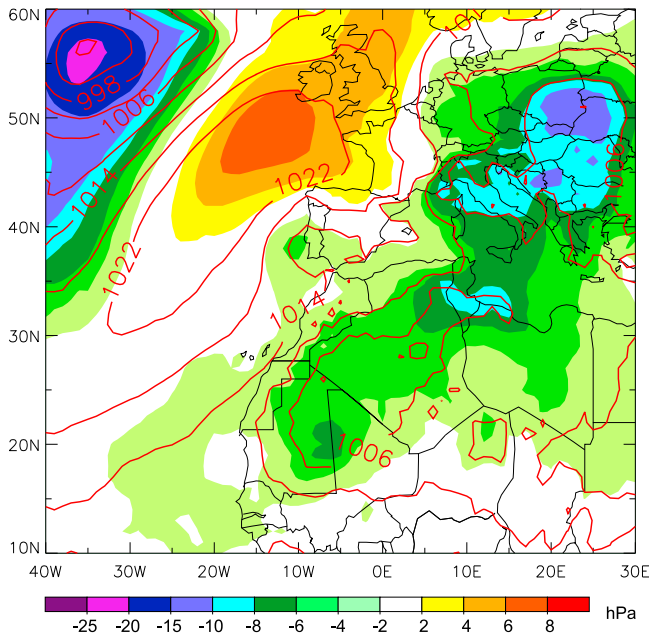


Figure 10. Same as Figure 7 but for 4 August 2006.

the boreal summer. In this paper, the complex physical mechanisms of dust emission and transport that create this dust hot spot have been investigated on the basis of a regression analysis relating daily time series of area-averaged satellite dust products to the analyzed atmospheric circulation and moist convective activity. This bulk statistical analysis is complemented with detailed examinations of carefully selected case study examples.

[43] The results show a clear relation between dustiness over the CWS on one hand and tropical AEW disturbances and synoptic activity in the subtropics on the other hand. The results confirm some of the key features of the idealized view of the great Saharan dust plumes proposed by *Karyampudi and Carlson* [1988] and *Karyampudi et al.* [1999] based on a more restricted analysis of case study events. Most notably, they suggest that dust generation occurs over the Sahara in the northeasterlies around the Saharan heat low when surface pressure gradients are enhanced by the passage of an AEW surface trough. This dust is then mixed throughout the Saharan Air Layer and transported out over the Atlantic in the easterly mid-tropospheric flow. Here we confirm the importance of the northeasterlies around the near-surface trough over the CWS but provide important additional detail, which illustrates the complexity of processes resulting in the CWS dust hot spot. The two important mechanisms that have not been documented previously are as follows.

[44] 1. During the 2–3 days before the peak in dustiness over the CWS region, a high-amplitude extratropical wave over northern Africa interacts with an AEW, leading to an extended region of low-level southerly flow upstream of and over the CWS, which in some cases mobilizes dust at the leading edge of the monsoon flow (mechanism D in section 1), but more importantly brings moisture into the southern Sahara. Moist convection that develops in this air mass is subject to considerable evaporation of hydrometeors in the usually extremely dry midlevel air over the desert. This

causes haboob dust storms as far north as the central Sahara (mechanism B). Over the following days this dust mixes through the deep Saharan boundary layer and eventually gets transported over the CWS region with the northerlies between the ridge and trough of the following AEW disturbance.

[45] 2. More dust emission can occur over the CWS itself in the associated northeasterly flow at the surface, in particular during the morning hours when momentum from nocturnal LLJs is mixed downward (mechanism C). Again, variations in the pressure distribution in the subtropics can enhance or even dominate this process as discussed by *Knippertz* [2008]. As such, the summertime CWS dust hot spot results from emissions from local sources and advection of dust generated to the east and north from a combination of large-scale and mesoscale processes involving a complex interplay between the tropical and the extratropical circulations. The fact that AEWs are often better organized and more strongly involved in the organization of moist convection to the west of the Greenwich Meridian [*Fink and Reiner*, 2003] supports the prominence of the CWS region.

[46] Our work presents the most comprehensive analysis of dust variability over the CWS region conducted to date. We utilize independent long-term satellite data sets from the TOMS/OMI and the MISR sensors. The results are to some degree sensitive to the employed data. The TOMS/OMI AI has a bias toward aerosols at higher elevation such that it is best in detecting dust loadings in the upper parts of the deep Saharan boundary layer, whilst MISR suffers from poor temporal sampling. Neither data set resolves dust loadings under cloud. The temporal resolution of the SEVIRI dust product facilitates much more detailed identification of dust sources [*Schepanski et al.*, 2009] but the qualitative information is not suitable for statistical analysis. There are at times large discrepancies between the SEVIRI dust product and the OMI AI that are probably related to problems of the former in detecting dust in humid air to the south of the ITD and to a sensitivity to particle size. Separating the limitations in these data is problematic and requires further work in the future, which should include the quantitative Moderate Resolution Imaging Spectroradiometer (MODIS) deep blue AOT estimates and lidar observations from CALIPSO. Generally the discrepancies between the different satellite products limit our ability to resolve the processes involved in more detail. This highlights the need for in situ observations of meteorological and aerosol processes in the CWS region. Previous field campaigns in the Sahara, including SHADE, AMMA, SAMUM, and GERBILS have been focussed on the periphery of the CWS. There is a clear need to fill this gap in our observational record.

[47] **Acknowledgments.** Part of this work was made possible through funding to the first author within the Emmy Noether program of the German Science Foundation DFG (grant KN 581/2–3). The authors are grateful to the ESSC at the University of Reading for access to SEVIRI dust product data through the Radagast project Web page. We would like to thank the three anonymous reviewers, whose thoughtful and constructive comments helped to improve an earlier version of the paper.

References

Ahn, C., O. Torres, and P. Bhartia (2008), Comparison of Ozone Monitoring Instrument UV aerosol products with Aqua/Moderate Resolution Imaging Spectroradiometer and Multiangle Imaging Spectroradiometer

- observations in 2006, *J. Geophys. Res.*, *113*, D16S27, doi:10.1029/2007JD008832.
- Ansmann, A., M. Tesche, P. Knippertz, E. Bierwirth, D. Althausen, D. Müller, and O. Schulz (2009), Vertical profiling of convective dust plumes in southern Morocco during SAMUM, *Tellus, Ser. B*, *61*, 340–353.
- Bothwell, G., E. Hansen, R. Vargo, and K. Miller (2002), The Multi-angle Imaging SpectroRadiometer science data system, its products, tools, and performance, *IEEE Trans. Geosci. Remote Sens.*, *40*(7), 1467–1476.
- Bou Karam, D., C. Flamant, P. Knippertz, O. Reitebuch, J. Pelon, M. Chong, and A. Dabas (2008), Dust emissions over the Sahel associated with the West African monsoon intertropical discontinuity region: A representative case-study, *Q. J. R. Meteorol. Soc.*, *134*, 621–634.
- Brooks, N., and M. Legrand (2000), Dust variability over northern Africa and rainfall in the Sahel, in *Linking Land Surface Change to Climate Change*, edited by D. McLarena and S. Kniverton, pp. 1–25, Kluwer Acad., Dordrecht, Netherlands.
- Burpee, R. (1974), Characteristics of North African easterly waves during the summers of 1968 and 1969, *J. Atmos. Sci.*, *31*, 1556–1570.
- Chaboureau, J.-P., P. Tulet, and C. Mari (2007), Diurnal cycle of dust and cirrus over West Africa as seen from Meteosat Second Generation satellite and a regional forecast model, *Geophys. Res. Lett.*, *34*, L02822, doi:10.1029/2006GL027771.
- Christopher, S., J. Haywood, and G. Greed (2008), Aerosol optical thicknesses over North Africa: 1. Development of a product for model validation using Ozone Monitoring Instrument, Multiangle Imaging Spectroradiometer, and Aerosol Robotic Network, *J. Geophys. Res.*, *113*, D00C04, doi:10.1029/2007JD009446.
- Davis, C., S. Jones, and M. Riemer (2008), Hurricane vortex dynamics during Atlantic extratropical transition, *J. Atmos. Sci.*, *65*, 714–736.
- Engelstaedter, S., and R. Washington (2007), Atmospheric controls on the annual cycle of North African dust, *J. Geophys. Res.*, *112*, D03103, doi:10.1029/2006JD007195.
- Engelstaedter, S., I. Tegen, and R. Washington (2006), North African dust emissions and transport, *Earth Sci. Rev.*, *79*, 73–100.
- Fink, A., and A. Reiner (2003), Spatio-temporal variability of the relation between African easterly waves and West African squall lines in 1998 and 1999, *J. Geophys. Res.*, *108*(D11), 4332, doi:10.1029/2002JD002816.
- Flamant, C., J.-P. Chaboureau, D. Parker, C. Taylor, J.-P. Cammas, O. Bock, F. Timouk, and J. Pelon (2007), Airborne observations of the impact of a convective system on the planetary boundary layer thermodynamics and aerosol distribution in the inter-tropical discontinuity region of the West African Monsoon, *Q. J. R. Meteorol. Soc.*, *133*, 1175–1189.
- Flamant, C., P. Knippertz, D. Parker, J.-P. Chaboureau, C. Lavaysse, A. Augusti-Panareda, and L. Kergoat (2009), The impact of a mesoscale convective system cold pool on the northward propagation of the inter-tropical discontinuity over West Africa, *Q. J. R. Meteorol. Soc.*, *135*, 139–159.
- Forster, P., et al. (2007), Changes in atmospheric constituents and in radiative forcing, in *Climate Change 2007: The Physical Science Basis. Contribution of Working Group I to the Fourth Assessment Report of the Intergovernmental Panel on Climate Change*, edited by S. Solomon et al., chap. 2, pp. 129–234, Cambridge Univ. Press, Cambridge, U. K.
- Haywood, J., P. Francis, M. Glew, and J. Taylor (2001), Optical properties and direct radiative effect of Saharan dust: A case study of two Saharan dust outbreaks using aircraft data, *J. Geophys. Res.*, *106*(D16), 18,417–18,430.
- Herman, J., and E. Celarier (1997), Earth surface reflectivity climatology at 340–380 nm from TOMS data, *J. Geophys. Res.*, *102*(D23), 28,003–28,011.
- Herman, J. R., P. Bhartia, O. Torres, C. Hsu, C. Seftor, and E. Celarier (1997), Global distribution of UV-absorbing aerosols from Nimbus 7/TOMS data, *J. Geophys. Res.*, *102*(D14), 16,911–16,922.
- Hsu, N., J. Herman, O. Torres, D. T. B. Holben, T. Eck, A. Smirnov, B. Chatenet, and F. Lavenue (1999), Comparisons of the TOMS aerosol index with Sun-photometer aerosol optical thickness: Results and applications, *J. Geophys. Res.*, *104*(D6), 6269–6279.
- Jickells, T., et al. (2005), Global iron connections between desert dust, ocean biogeochemistry, and climate, *Science*, *308*(5718), 67–71.
- Jones, C., N. Mahowald, and C. Luo (2003), The role of easterly waves on African desert dust transport, *J. Clim.*, *16*, 3617–3628.
- Kalnay, E., et al. (1996), The NCEP/NCAR 40-year reanalysis project, *Bull. Am. Meteorol. Soc.*, *77*, 437–471.
- Karyampudi, V., and T. Carlson (1988), Analysis and numerical simulations of the Saharan air layer and its effect on easterly wave disturbances, *J. Atmos. Sci.*, *45*, 3102–3136.
- Karyampudi, V., et al. (1999), Validation of the Saharan dust plume conceptual model using lidar, Meteosat, and ECMWF data, *Bull. Am. Meteorol. Soc.*, *80*, 1045–1075.
- Kiladis, G., and M. Wheeler (1995), Horizontal and vertical structure of observed tropospheric equatorial Rossby waves, *J. Geophys. Res.*, *100*(D11), 22,981–22,997.
- Kiladis, G., C. Thorncroft, and N. Hall (2006), Three-dimensional structure and dynamics of African Easterly Waves. Part I: Observations, *J. Atmos. Sci.*, *63*, 2212–2230.
- Knippertz, P. (2008), Dust emissions in the West African heat trough—The role of the diurnal cycle and of extratropical disturbances, *Meteorol. Z.*, *17*(5), 553–563.
- Koch, J., and N. O. Renno (2005), The role of convective plumes and vortices on the global aerosol budget, *Geophys. Res. Lett.*, *32*, L18806, doi:10.1029/2005GL023420.
- Lawson, T. (1971), Haboob structure at Khartoum, *Weather*, *26*, 105–112.
- Li, J., P. Zhang, T. Schmit, J. Schmetz, and W. Menzel (2007), Technical note: Quantitative monitoring of a Saharan dust event with SEVIRI on Meteosat-8, *Int. J. Remote Sens.*, *28*, 2181–2186.
- Liebmann, B., and C. Smith (1996), Description of a complete (interpolated) outgoing longwave radiation dataset, *Bull. Am. Meteorol. Soc.*, *77*, 1275–1277.
- Mahowald, N., and J. Dufresne (2004), Sensitivity of TOMS aerosol index to boundary layer height: Implications for detection of mineral aerosol sources, *Geophys. Res. Lett.*, *31*, L03103, doi:10.1029/2003GL018865.
- Marshall, J., D. Parker, C. Grams, C. Taylor, and J. Haywood (2008), Uplift of Saharan dust south of the intertropical discontinuity, *J. Geophys. Res.*, *113*, D21102, doi:10.1029/2008JD009844.
- Pierangelo, C., A. Chédin, S. Heilliette, N. Jacquinet-Husson, and R. Armante (2004), Dust altitude and infrared optical depth from AIRS, *Atmos. Chem. Phys.*, *4*, 1813–1822.
- Prospero, J., P. Ginoux, O. Torres, S. Nicholson, and T. Gill (2002), Environmental characterization of global sources of atmospheric soil dust identified with the NIMBUS 7 Total Ozone Mapping Spectrometer (TOMS) absorbing aerosol product, *Rev. Geophys.*, *40*(1), 1002, doi:10.1029/2000RG000095.
- Richardson, M., et al. (2007), Measurements of heterogeneous ice nuclei in the western United States in springtime and their relation to aerosol characteristics, *J. Geophys. Res.*, *112*, D02209, doi:10.1029/2006JD007500.
- Schepanski, K., I. Tegen, B. Laurent, B. Heinold, and A. Macke (2007), A new Saharan dust source activation frequency map derived from MSG-SEVIRI IR-channels, *Geophys. Res. Lett.*, *34*, L18803, doi:10.1029/2007GL030168.
- Schepanski, K., I. Tegen, M. Todd, B. Heinold, G. Bönisch, B. Laurent, and A. Macke (2009), Meteorological processes forcing Saharan dust emission inferred from MSG-SEVIRI observations of subdaily dust source activation and numerical models, *J. Geophys. Res.*, *114*, D10201, doi:10.1029/2008JD010325.
- Sokolik, I., O. Toon, and R. Bergstrom (1998), Modeling the radiative characteristics of airborne mineral aerosols at infrared wavelengths, *J. Geophys. Res.*, *103*(D8), 8813–8826.
- Sutton, L. (1925), Haboobs, *Q. J. R. Meteorol. Soc.*, *51*, 25–30.
- Todd, M., R. Washington, G. Lizcano, S. Ragvahan, and P. Knippertz (2008), Regional model simulations of the Bodélé low-level jet of northern Chad during BoDEX 2005, *J. Clim.*, *21*, 995–1012.
- Torres, O., P. Bhartia, J. Herman, A. Sinyuk, P. Ginoux, and B. Holben (2002), A long term record of aerosol optical depth from TOMS observations and comparison to AERONET measurements, *J. Atmos. Sci.*, *59*, 398–413.
- Torres, O., A. Tanskanen, B. Veihelmann, C. Ahn, R. Braak, P. K. Bhartia, P. Veeffkind, and P. Levelt (2007), Aerosols and surface UV products from Ozone Monitoring Instrument observations: An overview, *J. Geophys. Res.*, *112*, D24S47, doi:10.1029/2007JD008809.
- Uppala, S., D. Dee, S. Kobayashi, P. Berrisford, and A. Simmons (2008), Towards a climate data assimilation system: Status update of ERA-interim, *ECMWF Newsl.*, *115*, 12–18.
- Wald, A., Y. Kaufman, D. Tanré, and B.-C. Gao (1998), Daytime and nighttime detection of mineral dust over desert using infrared spectral contrast, *J. Geophys. Res.*, *103*(D24), 32,307–32,313.
- Washington, R., and M. Todd (2005), Atmospheric controls on mineral dust emission from the Bodélé depression, Chad: The role of the low level jet, *Geophys. Res. Lett.*, *32*, L17701, doi:10.1029/2005GL023597.
- Washington, R., M. Todd, N. Middleton, and A. Goudie (2003), Dust-storm source areas determined by the Total Ozone Monitoring Spectrometer and surface observations, *Ann. Assoc. Am. Geogr.*, *93*(2), 297–313.
- Washington, R., M. Todd, S. Engelstaedter, S. Mbainayel, and F. Mitchell (2006), Dust and the low-level circulation over the Bodélé depression, Chad: Observations from BoDEX 2005, *J. Geophys. Res.*, *111*, D03201, doi:10.1029/2005JD006502.
- Westphal, D., O. Toon, and T. Carlson (1988), A case study of mobilization and transport of Saharan dust, *J. Atmos. Sci.*, *45*, 2145–2175.

Williams, E. (2008), Comment on “Atmospheric controls on the annual cycle of North African dust” by S. Engelstaedter and R. Washington, *J. Geophys. Res.*, *113*, D23109, doi:10.1029/2008JD009930.

Williams, E., N. Nathou, E. Hicks, C. Pontikis, B. Russell, M. Miller, and M. Bartholomew (2008), The electrification of dust-lofting gust

fronts (“haboobs”) in the Sahel, *Atmos. Res.*, *91*, 292–298, doi:10.1016/j.atmosres.2008.05.017.

P. Knippertz, Institute for Climate and Atmospheric Science, School of Earth and Environment, University of Leeds, Leeds LS2 9JT, UK. (p.knippertz@leeds.ac.uk)

M. C. Todd, Department of Geography, University of Sussex, Chichester I Bldg., Rm. 301, Falmer, Brighton BN1 9QJ, UK. (m.todd@sussex.ac.uk)